Resonant Capture and Tidal Evolution in Circumbinary Systems: Testing the Case of Kepler-38

Resonant Capture and Tidal Evolution in Circumbinary Systems: Testing the Case of Kepler-38

F.A. Zoppetti,[1]⋆ C. Beaugé,[1,2] and A.M. Leiva[1]

[1] *Observatorio Astronómico, Universidad Nacional de Córdoba, Laprida 854, Córdoba X5000GBR, Argentina*
[2] *Instituto de Astronomía Teórica y Experimental, Universidad Nacional de Córdoba, Laprida 854, Córdoba X5000GBR, Argentina*

ABSTRACT
Circumbinary planets are thought to form far from the central binary and migrate inwards by interactions with the circumbinary disk, ultimately stopping near their present location either by a planetary trap near the disk inner edge or by resonance capture. Here, we analyze the second possibility, presenting a detailed numerical study on the capture process, resonant dynamics and tidal evolution of circumbinary planets in high-order mean-motion resonances (MMRs). Planetary migration was modeled as an external acceleration in an N-body code, while tidal effects were incorporated with a weak-friction equilibrium tide model. As a working example we chose Kepler-38, a highly evolved system with a planet in the vicinity of the 5/1 MMR.

Our simulations show that resonance capture is a high-probability event under a large range of system parameters, although several different resonant configuration are possible. We identified three possible outcomes: aligned librations, anti-aligned librations and chaotic solutions. All were found to be dynamically stable, even after the dissipation of the disk, for time-spans of the order of the system's age.

We found that while tidal evolution decreases the binary's separation, the semimajor axis of the planet is driven outwards. Although the net effect is a secular increase in the mean-motion ratio, the system requires a planetary tidal parameter of the order of unity to reproduce the observed orbital configuration. The results presented here open an interesting outlook into the complex dynamics of high-order resonances in circumbinary systems.

1 INTRODUCTION

As of 2017, the *Kepler* mission has discovered ten circumbinary planetary systems (Kepler-16[1], Kepler-34 and Kepler-35[2], Kepler-38[3], Kepler-47[4], Kepler-64[5], Kepler-413[6], Kepler-453 [7], Kepler-451[8] and Kepler-1647[9]). Host binary stellar systems are generally composed of stars of sub-solar masses, with mass ratios between ∼ 0.2 and ∼ 1. All binary components define compact systems with periods no longer than ∼ 40 days and a wide range of eccentricities, from quasi-circular orbits up to very eccentric cases (∼ 0.52). The planets surrounding them also have a diversity of characteristics: masses between a few tenth of terrestrial masses to ∼ 2 Jupiter-masses, and while many are located close to the binary (semimajor axis ratios ∼ 0.25) others are farther away with semimajor axes ratio reaching ∼ 0.004. Most planets orbit the binary in surprising circular orbits, except Kepler-413 (eccentricity ∼ 0.12) and Kepler-34 (eccentricity ∼ 0.18).

As expected, planet formation around compact binary

stars is more complex than for single stars. One of the main differences is the strong eccentricity excitation induced by the secondary star leading to high relative velocities between planetesimals and, consequently, to disruptive collisions (e.g. Paardekooper et al. 2012; Meschiari 2012; Lines et al. 2014). The primordial disk is also expected to be affected by the gravitational perturbations of binary, again leading to eccentric disks (Müller & Kley 2012; Marzari et al. 2013). Both these effects conspire to make in-situ formation extremely difficult. However, since the magnitude of the gravitational perturbations are a strong function of the semimajor axis ratio, planetary formation far from the stars appears much easier, following usual core-accretion models. This suggest that circumbinary planets could have formed farther out, and later migrated inward and stalled near their current orbits (Dunhill & Alexander 2013). In this scenario a mechanism that stops the inward migration is necessary.

Two mechanisms may be invoked to stall planetary migration: planetary traps generated by an inner disk cavity (e.g. Masset et al. 2006) and resonance trapping (Nelson 2003), both identified as a result of hydrodynamical simulations. Nelson (2003), in his pioneering work for Jovian-size circumbinary planets, found that resonance trapping appeared to be an effective stalling mechanism, although which

[1] Doyle et al. (2011),[2] Welsh et al. (2012),[3] Orosz et al. (2012), [4] Orosz et al. (2012), [5] Kostov et al. (2013),[6] Kostov et al. (2014) [7] Welsh et al. (2015), [8]Baran et al. (2015), [9] Kostov et al. (2016).

2   *F.A. Zoppetti et al.*

commensurability acted as the barrier seemed to depend on the binary eccentricity. In all cases, however, the resonances were of high order and first degree (i.e. mean-motion ratio ~ *j*/1).

Pierens & Nelson (2007) extended this study to planets in the Super-earth mass range, showing that these planets were usually stopped near the edge of the inner disk cavity. Curiously, the semimajor axis at which the planets stalled was very close to the 5/1 MMR with the binary but the authors could not find evidence that the protoplanets were effectively in resonance. More sophisticated cases in which accretion is included were discussed in Pierens & Nelson (2008). They found that MMR-capture was the main trapping mechanism. However, if post-capture planetary accretion was sufficiently large to form Jovian or Super-Jovian masses, the planet could be ejected from the commensurability leading to scattering or collision with the binary.

After the discovery of the first circumbinary planets by the *Kepler* mission, Pierens & Nelson (2013) attempted to explain the orbital architecture of Kepler-16, Kepler-34 and Kepler-35 systems, again using hydro-simulations to model the planet migration. They showed that the planets in these systems can migrate and end up in stable orbits close to the binary, but had difficulties in recreating their observed configurations. With a similar goal and method, Kley & Haghighipour (2014) attempted to explain the orbit of Kepler-38 by presenting an improved and extended disk model that included more realistic thermodynamics and boundary conditions. As before, they found that the binary carves a steep inner edge in the disk whose exact location is sensitive with respect to the disk and simulation parameters. A vital reference point is the location of the 5/1 MMR with the secondary star. If the inner edge of the disk occurs closer to the star, hydro-simulations lead to a resonance capture in the 5/1 MMR; conversely, if the disk gap extends further out, the planet did not reach the 5/1 commensurability but was trapped by the cavity's edge and remained close to its location throughout the simulation.

Of these two possibilities (resonance capture and planetary trap), Kley & Haghighipour (2014) clearly stated their preference for the second. They found that smaller values for the inner radius of the computational mesh led to a more extended disk gap, placing the cavity edge beyond the 5/1 resonance. Thus, they claimed that more realistic hydro-simulations should lead to planetary traps in non-resonant motion with the binary. This conclusion was additionally fueled by the fact that the current semimajor axis of the planet is not close to the resonance, but significantly displaced. Explicitly, the present day mean-motion ratio between the secondary star and the planet is ~ 5.61, a long way up from the 5/1 value.

While at first hand it may be difficult to imagine a scenario in which the orbit of the planet migrated outwards after the dissipation of the disk, the semimajor axis of the binary could in fact have decreased over time due to tidal effects. As the radius of the primary star is much larger than expected for a young main sequence star with the same mass, it is expected that the primary, and the system as a whole, is significantly evolved (Orosz et al. 2012). This fact, in addition to the scarce separation between the primaries for their corresponding masses and radii, allows us to infer that the

Table 1. System parameters for Kepler-38 (Orosz et al. 2012).

Body	Radius	m [$M_\odot$]	P [d]	a [AU]	e
m_{-1}	1.757 $R_\odot$	0.949			
m_0	0.272 $R_\odot$	0.249	18.7954	0.1469	0.1032
m_1	4.35 $R_\oplus$	?	105.595	0.4644	≤ 0.032

tidal effects may have played an important role in the past evolution of the system.

Tidal evolution of resonant planets around single stars have been analyzed recurrently in the past years (e.g. Papaloizou & Terquem 2010; Papaloizou 2011; Lithwick & Wu 2012; Delisle et al. 2012; Batygin & Morbidelli 2013; Delisle et al. 2014), all showing a slow divergence of the system away from exact commensurability as a function of time. The extent of the divergence is a strong function of the system parameters, especially the tidal coefficients Q_i', and may reach large values for Q_i' (Lee et al. 2013). On the other hand, tidal evolution in circumbinary systems has so far received little attention, and mainly focused on spin dynamics rather than on orbital evolution (Correia et al. 2016). Thus not much is known about the role of tidal evolution in defining the current orbital architecture of circumbinary systems.

This background invites us to revisit the dynamical problem of resonance trapping and tidal evolution for circumbinary planets as applied to a particular system: Kepler-38. Our aim is to test whether the combined effects of these two phenomena can explain the present day planetary eccentricity and mean-motion ratio with the secondary star. Since many of the crucial parameters (e.g. mass and tidal coefficients) are little constrained, our analysis will also be able to establish some limits for these parameters in order for the adopted scenario to work.

This paper is organized as follows. In Section 2 we discuss the present state and past tidal evolution of Kepler-38 binary in order to estimate the primordial orbital configuration of the binary. These primordial values are then used in Section 3 as starting points for a set of N-body simulations of the inwards migration and trapping of the planet in the 5/1 MMR. We also discuss the stability and resonant dynamics the captured orbits attain after the dispersal of the disk. Section 4 is devoted to the later tidal evolution of the complete (binary+planet) system up to the present day and which combination of system parameters are compatible with the observed configuration. Finally, in Section 5 we summarize the results and discuss their implications.

2   THE PRESENT AND PRIMORDIAL KEPLER-38 SYSTEM

The known physical and orbital characteristics of the present day Kepler-38 system are reproduced in Table 1, as obtained by Orosz et al. (2012). We denote the masses of the binary components as by m_{-1} and m_0 (with the convention $m_{-1} > m_0$) while m_1 is reserved for the planetary body. All orbital elements are given in the Jacobi reference frame.

The absence of noticeable planetary perturbations on the stars place an upper value for m_1 of ~ 120$m_\oplus$, although its actual value is probably much lower. Application of the semi-empirical fit by Mills & Mazeh (2017) to the planetary

radius yields a most probable value of $m_1 \simeq 8m_\oplus$. However, exoplanets with similar radii have measured masses in the range $m_1 \in [2, 20]m_\oplus$ associated to a large diversity of chemical compositions and internal densities. Thus, although the planetary mass is probably of the order of $10m_\oplus$, lower or even higher values are possible.

In addition to the parameters given in Table 1, Orosz et al. (2012) calculated the spectroscopic metallicity ([Fe/H]= −0.11, assumed equal for both stars) and the age T of the system. The age was estimated using both the effective temperature and the mass of the primary star and comparing isochrones in a $\log(g)$ - T_{eff} diagram from the Dartmouth series (Dotter et al. 2008). Results gave values of T between 7 and 13 Gyrs.

The large radius of m_{-1}, compared to its mass, points towards an evolved star leaving the main sequence. Thus, not only is the system expected to be old but the physical radius of the main star should also have changed significantly from its primordial value. In order to estimate $R_i(t)$ we repeated the comparison of the system parameters with the isochrones from the Dartmouth series. The isochrones were downloaded from the database *The Dartmouth Stellar Evolution Database*, which are freely accessible from `http://stellar.dartmouth.edu/~models/`. We adopted the measured metallicity of [Fe/H]= −0.11, [α/Fe]= 0 (scaled-solar) and the photometric system *UBV(RI)c+2MASS+Kepler* in the range $t \in [1, 13]$ Gyrs, the same values used by Orosz et al. (2012).

Results are shown in Figure 1. The top panel reproduces the upper plot in Figure 9 of Orosz et al. (2012), showing the current position of the primary and secondary star (this latter zoomed in a secondary plot) on the mass-radius diagram which were superimposed on the isochrones from the Dartmouth series. Due to the degeneration of the isochrones for low mass stars (such as m_0), we used m_{-1} to estimate the age of the system. The blue curve corresponds to the isochrone that best intersects the current position of the primary, corresponding to $T = 12.08$ Gyrs. Taking into account the errors in the determination of m_{-1}, we estimate the age of the system as $T = 12 \pm 2$ Gyr, in good agreement with the value calculated in Orosz et al. (2012).

Assuming no significant mass loss in the stars since they entered the main sequence stage, it is then possible to determine their radial evolution $R_i(t)$ from the intersection of each isochrone with the value corresponding to the stellar mass. From top panel of Figure 1, we can infer that the radial evolution of the secondary star m_0 should have been negligible. This result is well known for very low-mass star evolution: the lifetimes in the main sequence for this type of stars are much longer than the age of the system (Bowers & Deeming 1984) and no appreciable evolution in size is expected in this stage. For this reason, for the rest of our study we assume $R_0(t) = R_0 = 0.272M_\odot$. The primary star, on the other hand, suffered an important evolution in its radius, form a zero-time value of $R_{-1}(t = 0) \simeq 0.84R_\odot$ to its present value of $R_{-1}(t = T) \simeq 1.757R_\odot$. To obtain a smooth functional form for $R_{-1}(t)$ we fitted the data to a rational function of the form

$$\frac{R(t)}{R_\odot} = \frac{A + Ct + Et^2}{1 + Bt + Dt^2 + Ft^3}, \tag{1}$$

using a maximum likelihood technique. Expressing the time
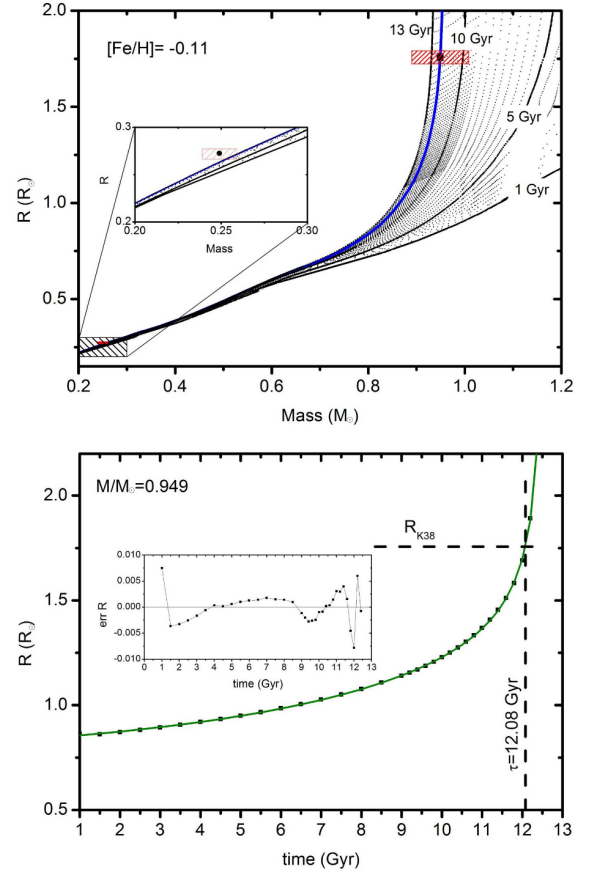
Figure 1. Top: Mass-radius diagram showing the present day values for the binary components of Kepler-38 (black circles) with their corresponding errors (red boxes), superimposed to the isochrones from the Dartmouth series (dotted lines) for the measured metallicity [Fe/H]= −0.11. The isochrones corresponding to 1, 5, 10 and 13 Gyrs have been highlighted in broad curves, while the isochrone that best intersects the position of the primary star is shown in blue (i.e. $T = 12.08$ Gyr). The secondary plot is a zoom around the position of the secondary mass. **Bottom:** Time evolution of the radius of the primary star (i.e. $R_1(t)$) (black dots) and the fitting rational function (green line). The dotted line corresponds to the current R_{-1} and the time estimated as the age of the system. The secondary plot shows the difference between the data and the values predicted by the fitting algorithm.

t in Gyrs, the resulting coefficients acquire values:

$$A = 8.402 \times 10^{-1} \quad ; \quad B = -1.205 \times 10^{-1}$$
$$C = -8.662 \times 10^{-2} \quad ; \quad D = 2.837 \times 10^{-3} \tag{2}$$
$$E = 1.662 \times 10^{-3} \quad ; \quad F = 3.530 \times 10^{-4}.$$

The bottom panel in Figure 1 shows the radial evolution of the primary star $R_{-1}(t)$ obtained from the isochrones, and the fitting rational function from equation (1). Notice that the size of this star has begun to evolve recently (~ 3 Gyr ago), when it began to leave the main sequence.

With this information in hand, we may now estimate the past orbital evolution of the system due to tidal interactions. We assume that both stars evolved in isolation but very quickly attained pseudo-synchronous spin rates. Adopting a Mignard-type equilibrium tide model (e.g. Mignard 1979; Hut 1981), the differential equations governing the

4   F.A. Zoppetti et al.
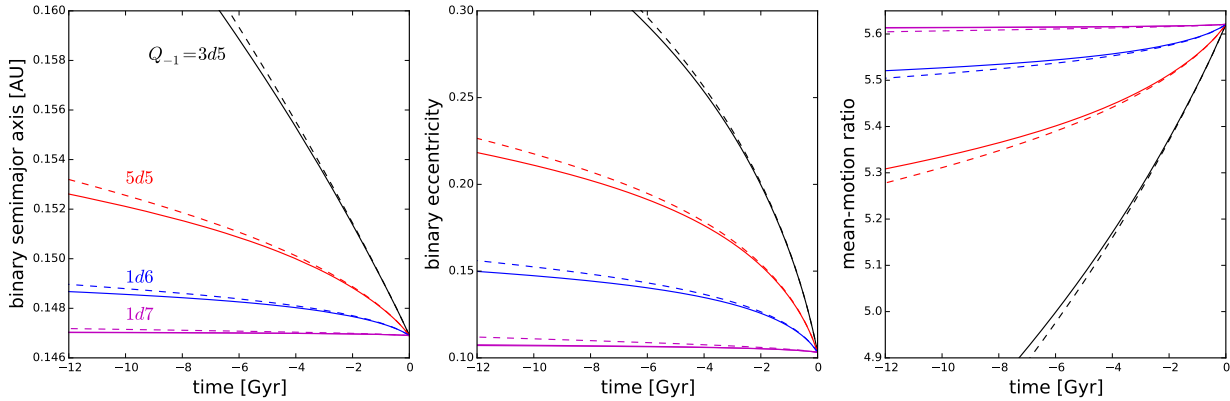
Figure 2. Past tidal evolution of the mean binary semimajor axis a_0 (left), mean binary eccentricity e_0 (middle), and mean-motion ratio n_0/n_1 (right), for different values of the tidal dissipation parameters. Continuous lines correspond to $Q'_0 = Q'_{-1}$ while broken lines show results assuming $Q'_0 = 10^5$ independently of the value of Q'_{-1}. The mean motion of the planet (i.e. n_1) was kept constant and equal to its current value.

time evolution of the mean binary semimajor axis a_0 and eccentricity e_0 may be written as:

$$\frac{1}{a_0}\frac{da_0}{dt} = -n_0 D_a(e_0)\left[\frac{1}{Q'_{-1}}\left(\frac{m_0}{m_{-1}}\right)\left(\frac{R_{-1}}{a_0}\right)^5 + \frac{1}{Q'_0}\left(\frac{m_{-1}}{m_0}\right)\left(\frac{R_0}{a_0}\right)^5\right]$$

$$\frac{1}{e_0}\frac{de_0}{dt} = -n_0 D_e(e_0)\left[\frac{1}{Q'_{-1}}\left(\frac{m_0}{m_{-1}}\right)\left(\frac{R_{-1}}{a_0}\right)^5 + \frac{1}{Q'_0}\left(\frac{m_{-1}}{m_0}\right)\left(\frac{R_0}{a_0}\right)^5\right]$$

$$(3)$$

where $D_a(e)$ and $D_e(e)$ may be written in terms of the classical eccentricity functions $f_i(e)$ as

$$D_a(e) = 9\left(f_3(e) - \frac{f_2^2(e)}{f_1(e)}\right)$$

$$D_e(e) = \frac{81}{2}\left(f_5(e) - \frac{11}{18}\frac{f_2(e)f_4(e)}{f_1(e)}\right),$$

$$(4)$$

with

$$f_1(e) = \frac{1 + 3e^2 + 3e^4/8}{(1-e^2)^{9/2}}$$

$$f_2(e) = \frac{1 + 15e^2/2 + 45e^4/8 + 5e^6/16}{(1-e^2)^6}$$

$$f_3(e) = \frac{1 + 31e^2/2 + 255e^4/8 + 185e^6/16 + 25e^8/64}{(1-e^2)^{15/2}}$$

$$f_4(e) = \frac{1 + 3e^2/2 + e^4/8}{(1-e^2)^5}$$

$$f_5(e) = \frac{1 + 15e^2/4 + 15e^4/8 + 5e^6/64}{(1-e^2)^{13/2}},$$

$$(5)$$

(e.g. Mignard 1980; Hut 1981; Correia et al. 2011). Expressions (3) are valid only in the case where both bodies are tidally locked.

We now apply these equations to the case of Kepler-38 binary. Given the present orbit, we wish to estimate the primordial values of a_0 and e_0 at the time of the dispersal of the proto-planetary disk. To do this, we must perform a back integration of the tidal equations for the age of the system, assuming the current values as initial conditions and taking into account the change in the radius of the primary star. The values of the stellar tidal parameters Q'_i are little

known, with estimates as low as 10^5 (e.g. Essick & Weinberg 2016; Maciejewski et al. 2016) and as high as 10^7 (Benítez-Llambay et al. 2011). We will consequently consider them as free parameters in our simulations.

Figure 2 shows the back evolution of the mean semi-major axis a_0 (left) and the eccentricity e_0 (middle plot) of the binary, over a total timespan of 12 Gyr and for four representative values of Q'_{-1}, indicated within the left-hand frame. Continuous lines show results with $Q'_0 = Q'_{-1}$, while broken lines correspond to $Q'_0 = 10^5$ for all values of Q'_{-1}. This latter case explores the possibility that the secondary star (with much larger mass density) could have a lower tidal parameter than its more massive companion. However, as seen here, there is no substantial difference in the results and the tidal evolution of the system is primarily dominated by tides raised on the central star.

As expected, tidal evolution implies that the primordial orbit of the binary must has been wider and more eccentric. Dissipation parameters $Q'_{-1} \lesssim 3 \times 10^5$ leads to divergent solutions and thus appear inconsistent with the present state of the binary. On the other extreme, practically no orbital change is observed for $Q'_{-1} \gtrsim 10^7$. In all cases, most of the orbital evolution appears to have occurred in the last few Gyrs, and is associated to the inflation of the physical radius of the primary stellar component.

The right-hand frame of Figure 2 shows the evolution of the mean-motion ratio n_0/n_1 between the binary and the planet, where for this analysis we have assumed no change in the value of n_1. Since stronger tidal effects imply larger initial values of a_0, the proximity of the primordial system to the 5/1 MMR could have been much smaller in the past. In particular, for $Q'_{-1} \sim 4 \times 10^5$ the original configuration of the system could have been quite close to the exact resonance and migrated out to the present value just by tidal evolution of the binary system without change in the planetary orbit. However, as we will see further on, large values for the initial eccentricity e_0 are not compatible with a smooth tidal ejection of the complete system (binary + planet) out of the commensurability.

3 MIGRATION AND RESONANT CAPTURE IN THE KEPLER-38 SYSTEM

We now add the planet m_1 to the dynamical system and adopt a Jacobi reference frame for the coordinates and velocities. The position vector $\vec{r}_0$ of the secondary star m_0 is then defined as m_{-1}-centric while the position vector $\vec{r}_1$ of the planet m_1 is measured with respect to the center of mass of m_{-1} and m_0. The planet's orbit, considered coplanar with the binary, will be characterized by its semimajor axis a_1, eccentricity e_1, mean longitude λ_1 and longitude of pericenter, all calculated from the Jacobi state vectors. Similar notation, but with subindex 0 will be used for the orbit of the secondary star m_0 around the primary star m_{-1}.

3.1 Resonant Structure

Let us now suppose that m_1 lies in the vicinity of a generic $(p+q)/p$ mean-motion resonance with the perturber m_0, such that

$$(p+q)n_1 - pn_0 \simeq 0 \tag{6}$$

where both p and q are positive integers. All resonant terms of the Hamiltonian normal form will then have the generic form

$$\phi_{res} = u(p+q)\lambda_1 - up\lambda_0 + j_2\varpi_0 + j_4\varpi_1 \tag{7}$$

where u is an integer defining the harmonic order of the resonant term, while D'Alambert's condition implies $j_2 + j_4 = -uq$. Considering the lowest-order harmonic ($u = 1$), we obtain $j_2 = k - (p+q)$ and $j_4 = p - k$ with k an integer.

Since the strength of a given resonant harmonic is proportional to $e_0^{|j_2|}e_1^{|j_4|}$, the set of independent resonant angles with the lowest order in eccentricity will be associated to values of k in the range $k \in [p, p+q]$. Thus, the resonant set that characterizes the $(p+q)/p$ resonance will contain $(q+1)$ independent resonant arguments of the form

$$\phi_{(p+q)/p}^{(l)} = (p+q)\lambda_1 - p\lambda_0 - q\varpi_0 - l(\varpi_1 - \varpi_0) \tag{8}$$

where $l = (k - p) \in [0, q]$. In the particular case of the 5/1 MMR, all lowest-order resonant terms of the disturbing function will contain one of the following possible critical arguments:

$$\phi_{5/1}^{(0)} = 5\lambda_1 - \lambda_0 - 4\varpi_0$$

$$\phi_{5/1}^{(1)} = 5\lambda_1 - \lambda_0 - 3\varpi_0 - \varpi_1$$

$$\phi_{5/1}^{(2)} = 5\lambda_1 - \lambda_0 - 2\varpi_0 - 2\varpi_1 \tag{9}$$

$$\phi_{5/1}^{(3)} = 5\lambda_1 - \lambda_0 - \varpi_0 - 3\varpi_1$$

$$\phi_{5/1}^{(4)} = 5\lambda_1 - \lambda_0 - 4\varpi_1,$$

which, from equation (8), may also be written succinctly as

$$\phi_{5/1}^{(l)} = \sigma - l\Delta\varpi \quad \text{where} \quad \sigma = (p+q)\lambda_1 - p\lambda_0 - q\varpi_0 \tag{10}$$

and $\Delta\varpi = \varpi_1 - \varpi_0$ is the difference in longitudes of pericenter.

While high-order MMRs are usually negligible in planetary systems around single stars, this is not the case for binary systems where the perturbing mass is comparable to the central mass (e.g. Leiva et al. 2013). Moreover, in
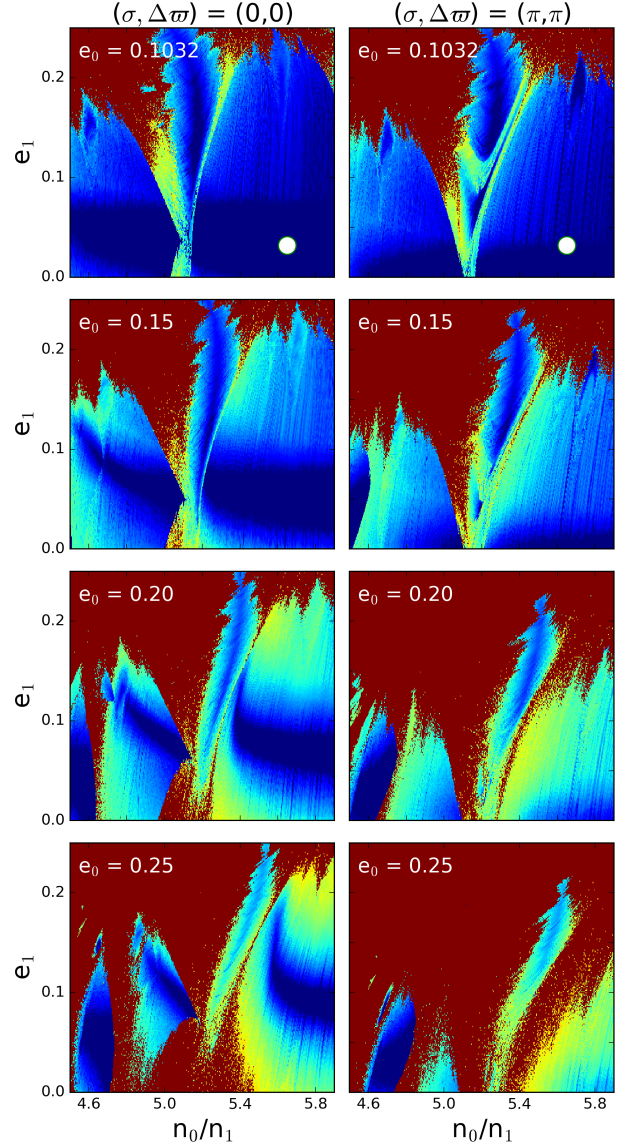
Figure 3. Dynamical maps in the $(n_0/n_1, e_1)$ plane with different values of the binary eccentricity e_0 and initial angles leading to $(\sigma, \Delta\varpi) = (0, 0)$ (left-hand plots) and $(\sigma, \Delta\varpi) = (\pi, \pi)$ (right-hand column). Blue (red) tones correspond to low (high) values of $\max(\Delta e)$, respectively. Total integration time was 10^3 years.

the case of circumbinary planets the $j/1$ commensurabilities appear as the strongest and more isolated resonances (Gallardo 2006), and thus the most likely final destination through planetary migration.

Preliminary N-body simulations of the capture and dynamical evolution of systems within the 5/1 MMR showed that all stable resonant solutions cross one of two representative planes: one represented by values of the angles $(\sigma, \Delta\varpi) = (0, 0)$ corresponding to aligned orbits, and a second plane with $(\sigma, \Delta\varpi) = (\pi, \pi)$, this time corresponding to anti-aligned configurations. Although asymmetric solutions are expected for exterior $j/1$ resonances (e.g. Beaugé 1994), here these seem to be associated to high eccentricities and have not been found in any of our simulations.

6   *F.A. Zoppetti et al.*

Figure 3 shows a set of dynamical maps in the $(n_0/n_1, e_1)$ plane. Each frame shows a map for a 400×200 grid of initial conditions, each integrated for a total timespan of 10^3 years. The color code indicates the maximum change in the planetary eccentricity during the integration timespan, usually referred to as the max(Δe)-indicator (e.g. Ramos et al. 2015). The planetary mass was taken equal to $m_1 = 120 m_\oplus$, although no significant difference was noted in the maps when using smaller masses. Initial values for the angles correspond to $(\sigma, \Delta\varpi) = (0, 0)$ for the left-hand graphs and $(\sigma, \Delta\varpi) = (\pi, \pi)$ for the right-hand column.

The present day location of the planet is indicated with a large white filled circle in the two top frames, both drawn for the current value of the binary eccentricity. While no reliable information is available for the observed $\Delta\varpi$, the current upper value for the eccentricity is very close to the Mode I secular mode (e.g. Michtchenko & Malhotra 2004) corresponding to aligned orbits. This secular mode is visible for all binary eccentricities, although increasingly distorted by the expanding libration domain of the mean-motion resonances.

Up to moderate values of e_1 (i.e. ~ 0.20), the structure of the 5/1 resonance is clearly visible as a classical V-shape librational domain. A wide chaotic layer dominates the left-hand separatrix and weaker counterpart may be seen in the right side. However for $e_0 \gtrsim 0.2$ both branches generate a strong chaotic layer separating the resonant from non-resonant domains. In all cases, however, the inner librational region still shows an inner core of more regular motion, whose location with respect to the exact resonance increases with the binary eccentricity.

3.2   Ad-hoc Planetary Migration

Simulating the whole process of disk-induced migration in the circumbinary environment is beyond the scope of the present paper. We instead opted to add to a N-Body integrator an ad-hoc external acceleration that mimics the migration mechanisms that the hydrosimulations show. This technique is well documented for planetary systems around single stars (e.g. Lee & Peale 2002; Beaugé et al. 2006; Cresswell & Nelson 2008), and was recently used to study scattering processes between circumbinary planets and the binary system by Rodet et al. (2017). It is generally believed that circumbinary disks may present different properties respect to disks around simple stars, so the migration processes may also be different. However, since the principal aim of this section is to analyze the dynamical capture into resonance, usual ad-hoc prescriptions for planetary migration will be used.

We assume that the protoplanetary disk was symmetric with respect to the center of mass of the binary, thus prompting the use of a Jacobi reference frame for the complete system. The gaseous disk was considered thin and laminar with a power-law dependence for both the surface density $\Sigma(r) = \Sigma_0 \, r^\gamma$ and aspect ratio $H_r(r) = H_0 \, r^f$. Their values at $r = 1$ was set to $\Sigma_0 = 1 \times 10^{-5}$ M$_\odot$/ AU^2 and $H_0 = 0.05$. The exponents were taken equal to $\gamma = 1/2$ and $f = 0$, this last value corresponding to a flat disk.

Following Cresswell & Nelson (2008), the acceleration of the planet due to the interaction with the disk was modeled

by an exterior non-conservative term defined by

$$\ddot{\vec{r}}_1 = -\left[\frac{\vec{v}_1}{2\tau_a} + 2\frac{(\vec{v}_1 \cdot \vec{r}_1)\vec{r}_1}{r_1^2 \, \tau_e} \right] \tag{11}$$

where $\vec{v}_1$ is the Jacobi velocity vector of the planet while τ_a and τ_e are the orbital migration and eccentricity damping timescales, respectively. No disk-induced migration was considered for the secondary star.

From linear models (e.g. Tanaka & Ward 2004; Cresswell & Nelson 2008), in the low eccentricity limit we may write

$$\tau_a = Q_a \frac{t_{wave}}{H_r^2} \qquad ; \qquad \tau_e = Q_e \frac{t_{wave}}{0.780} \tag{12}$$

where the quantity Q_e is an ad-hoc constant parameter introduced by Cresswell & Nelson (2006) to fit the results of hydrodynamical simulations. They found that the best results were obtained with $Q_e = 0.1$, a value that we also adopt here. On the other hand, $Q_a = Q_a(\gamma)$ is a function of the slope of the surface density profile which, from Tanaka et al. (2002), is given by $Q_a^{-1} \simeq 2.7 + 1.1\gamma$. While numerical fits with hydrosimulations sometimes lead to slightly different functional forms (e.g. D'Angelo & Lubow 2010), here we adopted the classical expression. The typical timescale t_{wave} for planetary migration is given by

$$t_{wave} = \frac{M_B^2 H_r^2}{m_1 n_1 a_1^2 \Sigma(a_1)} \tag{13}$$

where $M_B = m_{-1} + m_0$ is the total mass of the binary.

Finally, we consider the modifications of Goldreich & Schlichting (2014) to take into account the contribution of eccentricity damping to changes in the semimajor axis associated with partial conservation of the angular momentum. Thus, the effective characteristic timescale for orbital migration should actually be given by

$$\frac{1}{\tau_{a_{eff}}} = \frac{1}{\tau_a} + 2\beta \frac{e_1^2}{\tau_e} \tag{14}$$

where τ_a and τ_e maintain the same form as Equations (12) and β is a factor that quantifies the fraction of the orbital angular momentum preserved during the migration. Goldreich & Schlichting (2014) refer to estimations by Tanaka & Ward (2004) that suggest $\beta = 0.3$ for Type-I disk-planet interactions.

We performed a series N-Body simulations of planetary migration in circumbinary disks using this simple analytical prescription, to which we also added relativistic effects, modeled following the post-Newtonian formulation of Richardson & Kelly (1988). The initial semimajor axis for the planet was chosen beyond the 6/1 MMR with the binary, $e_1 = 0.05$ and all angles set to zero. In all cases, we assumed that the planet was already formed when the migration began and that there was no additional accretion. Each run was followed for a total timespan of 10^5 yrs (roughly 2×10^6 binary periods) to study the long-term evolution. The surface density was artificially decreased down to zero in the time interval $t \in [6 \times 10^4, 8 \times 10^4]$ years following a linear trend. This interval was sufficiently long for the transition to be adiabatic with respect to the resonant and secular timescales. The last 20% of the simulation thus occurred without the effects of non-conservative forces, ensuring that
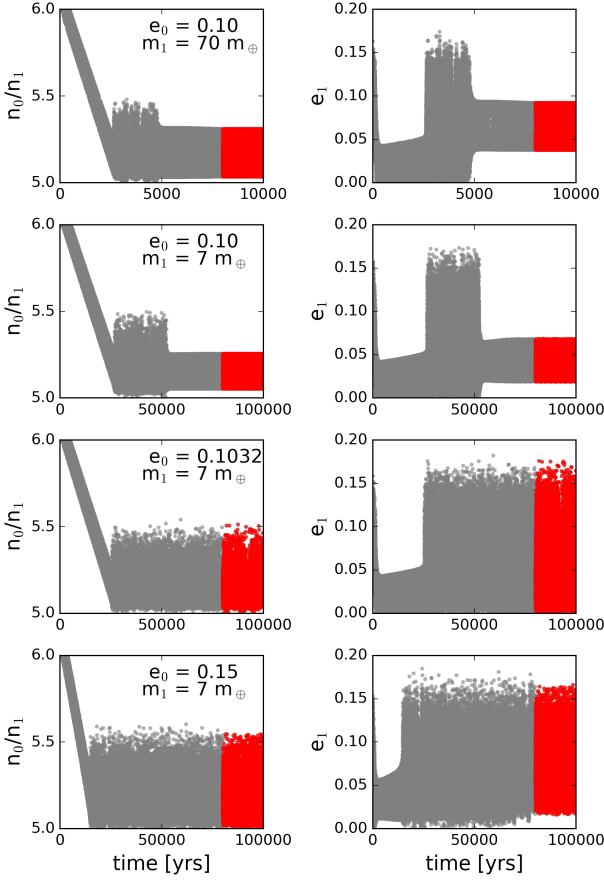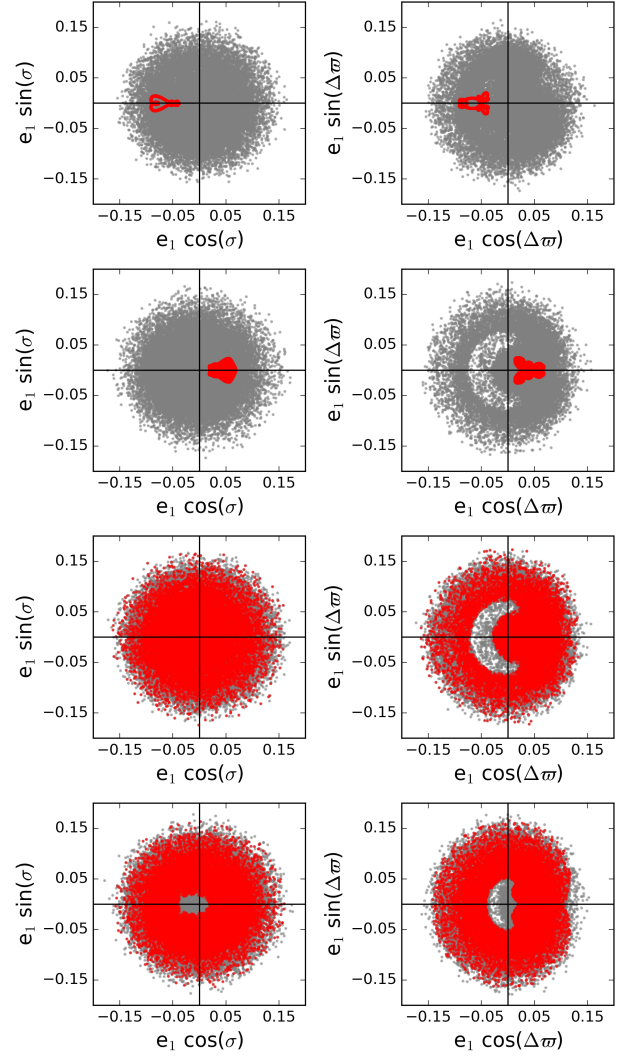
Figure 4. Evolution of the mean-motion ratio n_0/n_1 (left) and planetary eccentricity (right) during planetary migration and capture in the 5/1 MMR for four different values of (e_0, m_1). The time interval prior to the dispersal of the disk is shown in gray dots while the resonant dynamics stemming from the purely gravitational interactions is highlighted in red. For $m_1 = 70 m\oplus$ the migration and disk dissipation timescales was accelerated by a factor 10 with respect to the smaller masses.

Figure 5. Orbital evolution in the regular variables $(k_\sigma, h_\sigma) = (e\cos\sigma, e\sin\sigma)$ (left columns) and $(k_{\Delta\varpi}, h_{\Delta\varpi}) = (e\cos\Delta\varpi, e\sin\Delta\varpi)$ (right column) for the simulations described in Figure 4. The time interval prior to the dispersal of the disk is shown in gray dots while the resonant dynamics stemming from the purely gravitational interactions is highlighted in red.

the final configuration was stable and representative of the dynamics in a gas-free scenario.

Due to the lack of information of the planetary mass, we ran simulations in the range $m_1 \in [1, 120]m\oplus$. Prompted by the backwards tidal evolution, we considered primordial binary eccentricities in the range $e_0 \in [0.10, 0.25]$. This value was kept constant throughout the migration. While resonant capture in the 5/1 MMR were also found for higher values of e_0, most initial conditions led to orbital instabilities as soon as the eccentricity damping force was decreased to zero. This seems to indicate a minimum value for the tidal parameter of the central star of the order of $Q'_{-1} \gtrsim 5 \times 10^5$ for resonant capture to have been probable in the original configuration of the Kepler-38 system.

Depending on the values of e_0 and m_1 we found three possible final outcomes for planets trapped in the 5/1 mean-motion resonance; their dynamical behavior is summarized in Figures 4 and 5. The first presents the evolution of the mean-motion ratio n_0/n_1 and the eccentricity of the planet e_1 during the migration process and after the dissipation

of the disk. While only four cases are shown, these proved the only types found in our analysis of the parameter space. Masses and values of e_0 are specified in the left-hand column. Figure 5 shows the behavior of the primary resonant and secular angles (see equation (10)). These are plotted in regular variables with the planetary eccentricity e_1 as the radial distance. Results obtained during the disk lifetime are shown in gray while those after disk dispersal are depicted in red.

Upon reaching the 5/1 resonance, all initial conditions enter a chaotic region which seems to be associated to an outer separatrix of the commensurability (see Figure 3). This is seen in Figure 4 as a large-amplitude oscillation in both the semimajor axis and eccentricity. We found that for $e_0 \leq 0.10$ this phase is temporary and the planet ultimately enters a more regular inner resonant region in which all resonant

8   F.A. Zoppetti et al.

angles librate. Depending on the planetary mass, the center of libration may correspond to $(\sigma, \Delta\varpi) = (\pi, \pi)$ (as shown for $m_1 = 70m_\oplus$) or to $(\sigma, \Delta\varpi) = (0,0)$, as seen for $m_1 = 7m_\oplus$. This second mode corresponds to a libration of all critical angles (9) around zero, while in the first (anti-aligned) mode the critical angles librate around zero or π depending on the multiplicity of the longitude of pericenter.

The anti-aligned mode seems to be preferred by large planetary masses while small values of m_1 always seem to be trapped in an aligned mode. However, the precise limit appears to be a strong function of the binary eccentricity and a more in-depth analysis of this behavior is still pending.

For $e_0 > 0.10$, the planet does not seem able to pass into the inner libration domain of the 5/1 MMR and exhibits large, apparently chaotic, oscillations in semimajor axis and eccentricity, even after the dispersal of the disk. In most cases this is accompanied by a lack of librations of the resonance angles, although we did note a few examples where $\phi_{5/1}^{(3)}$ librated around zero. This behavior is similar to that noted by Kley & Haghighipour (2014) in their hydrosimulations, although in our case it was only observed for larger binary eccentricities. The chaoticity was checked in additional runs without the relativistic effects, and is probably linked to the overlap of different sub-resonances, each associated to a different critical angle.

Notwithstanding the different dynamical evolutions, all these simulations proved to be dynamically stable, even after extending the total integration time to over 10^9 orbital periods of the binary. This seems to indicate that librations of the resonant angles are not a necessary condition for resonance capture, at least for the present problem.

4   TIDAL EVOLUTION TO THE CURRENT KEPLER-38 SYSTEM

Having established the conditions for trapping and final orbital configurations for the system after the dissipation of the primordial disk, the next (and final) step is to study its later evolution up to the present day. In a gas-free environment the only interacting forces are gravitational, and these include the tidal interactions of the complete (binary+planet) system.

Since we lack an adequate analytical model for the 5/1 MMR, we opted for a pure N-body approach in which the tidal forces were modeled following Mignard (1979) as applied in (e.g. Rodriguez et al. 2011; Beaugé & Nesvorný 2012). As described in Section 2, we incorporated into the N-body code the temporal evolution in the radius of the primary star; the secondary suffered negligible change and was assumed constant. The whole system was then integrated for a timespan equivalent to the age of the system, set as before at $T = 12$ Gyrs. Since this timespan corresponds to about 10^{12} orbital periods of the binary, numerical integrations for nominal values of the system parameters proved prohibited. Consequently, we scaled down the total timespan and the tidal parameters by an identical factor $\gamma > 1$ to reduce the integration time to reasonable levels.

In the case of non-interacting masses in pseudo-synchronous configurations, the scaling of both time and tidal parameters leads to the same orbital evolution, regardless of the value of γ. The same, however, does not hold

when mutual gravitational interactions are introduced, potentially leading to spurious results in the accelerated system. In order to guard against this possibility, we considered only values of γ sufficiently low to maintain the accelerated tidal evolution adiabatic with respect to the resonant and secular gravitational timescales. Following preliminary tests we adopted $\gamma = 10^5$, although, as an additional security measure, we repeated some runs with lower values to guarantee reliable results.

The current location of the Kepler-38 planets corresponds to $(n_0/n_1, e_1) \simeq (5.61, 0.03)$, with the mean-motion ratio a long way up from the average value found in our capture simulations ($n_0/n_1 \simeq 5.2$). Although for high binary eccentricities we were able to find solutions with osculating values up to ~ 5.6, these instants are accompanied by maxima of the planetary eccentricity ($e_1 \simeq 0.15 - 0.2$) and thus inconsistent with present-day values. It thus appears that the only possibility in explaining the Kepler-38 system after a 5/1 MMR capture is through a strong tidal evolution leading to an ejection from the resonance and a subsequent secular drift up to the observed separation.

Here lies our first problem. Once spin-orbit equilibrium is reached and the planet leaves the resonant domain, tidal dissipation is expected to lead to a decrease in the semimajor axes (see equation (5)). Thus, in order for the mean-motion ratio n_0/n_1 to increase up to current values, in principle it is necessary for the semimajor axis of the binary to decrease faster than that of the planet and by a significantly larger amount. As seen from the right-hand frame of Figure 2, this condition implies that the tidal parameter of the central star must be $Q'_{-1} \lesssim 5 \times 10^5$, or even lower if the planetary tidal evolution was important. Adopting lower values for Q'_0 does not seem to modify the problem significantly.

Although such values are consistent with some estimations (e.g. Maciejewski et al. 2016), they imply primordial eccentricities for the binary $e_0 \gtrsim 0.25$ (middle frame of Figure 2). Not only is then resonance capture a low probability event, but the outcome of the subsequent tidal evolution always appears to be close encounters and disruption of the system. This instability is believed to be caused by the enhanced chaotic layer delimiting the different sub-resonant domains, and is more pronounced in the inner separatrix of the commensurability. Even if the large stochastic region may be crossed successfully under the effects of a relatively fast planetary migration, tidal evolution is much slower, giving time for the intrinsic instabilities to act and ultimately drive the planet into a crossing orbit with the secondary star.

These dynamical constraints seem to indicate a larger value for the tidal parameter of the central star, of the order of $Q'_{-1} \gtrsim 10^6$, leading to a lower initial binary eccentricity and a much less prominent chaotic layer (see Figure 3). The problem here lies in that the tidal decay of the binary would not be sufficient to account for the current value of n_0/n_1. Consequently, most of the divergent migration must have come from the tidal evolution of the planet itself. This raises two issues: (i) whether the planetary tide could have been strong enough for the required migration scale, and (ii) whether the direction of the tidal migration could in fact been outwards and not inwards as expected from secular dynamics.
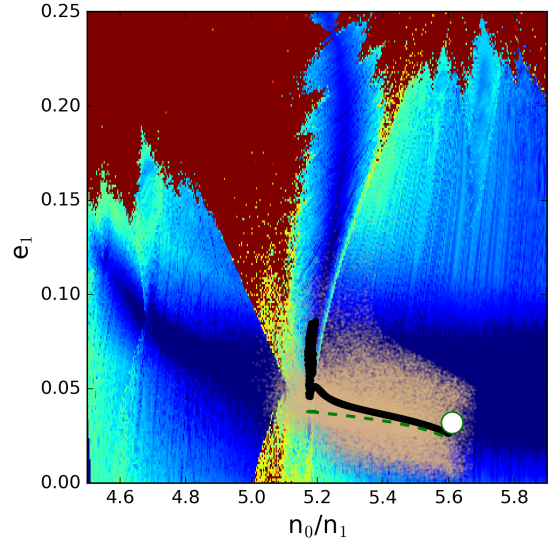
Figure 6 shows the results of an N-body simulation
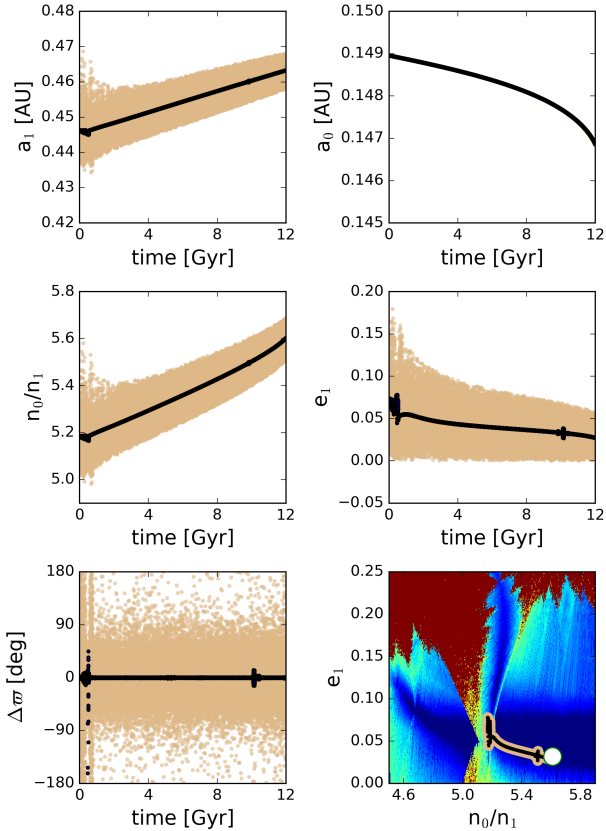
Figure 6. N-body simulation of the tidal evolution of a $m_1 = 2m_\oplus$ planet initially trapped in the 5/1 MMR with the binary ($e_0 = 0.156$). Tidal parameters were chosen equal to $Q'_{-1} = 10^6$, $Q'_0 = 10^5$ and $Q'_1 = 10/3$. Brown dots show osculating orbital elements while black lines correspond to filtered values, averaged over short period terms. The white circle in the lower right-hand plot is the current location of Kepler-38 in the ($n_0/n_1, e_1$) plane.

Figure 7. Results of a second N-body simulation, this time adopting $m_1 = (20/3)\,m_\oplus$ and $Q'_1 = 1$, while all other system parameters were kept equal as those used in Figure 6. Light brown dots correspond to osculating elements while orbitally-averaged values are shown as a thick black curve. The dashed green curve is the forced eccentricity as given by equation (15). The current location of Kepler-38 is indicated by a filled white circle.

mimicking the tidal evolution of a $m_1 = 2m_\oplus$ planet, initially trapped in the 5/1 MMR, for a timespan equivalent to the system's age. Tidal parameters for the stars were taking equal to $Q'_{-1} = 10^6$ and $Q'_0 = 10^5$, implying that the initial eccentricity of the binary was $e_0 = 0.156$. The tidal parameter for the planet was assumed to be $Q'_1 = 10/3$ and its physical radius equal to the observed value. The brown dots show the osculating orbital element, while the black curves correspond to values obtained after applying a FIR-type digital filter (e.g. Carpino et al. 1987) to eliminate the short-period variations.

The two top frames show the time evolution of the semimajor of the planet (left) and the secondary star (right). While a_0 decreases as a function of time, as expected from the tidal equations (3), the planet's semimajor axis has the inverse behavior and increases with time. Without a reliable model for the MMR it is not possible to establish if this effect is caused by the resonant structure, but this explanation appears improbable since we would not expect its effect to reach beyond the immediate vicinity of the commensurability.

A second, more likely explanation, may lie in the effects of the near-resonant terms on the secular aligned-mode,

whose forced eccentricity grows considerably close to the inner separatrix. Since tidal effects are dominated by eccentricity damping, then perhaps the system follows the perturbed secular aligned-mode outwards from the exact commensurability which, instead of causing a decrease in semimajor axis, leads outwards. This hypothesis is supported by the behavior of e_1 and $\Delta\varpi$ in Figure 6, showing the planet rapidly entering the secular aligned-mode as soon as it leaves the resonance and evolving towards more circular orbits as the mean-motion ratio n_0/n_1 increases up to values close to the current location of the planet. However, additional studies are necessary before we can prove this idea with any certainty.

Finally, the lower right-hand frame of the figure shows the escape route of the system in the ($n_0/n_1, e_1$) plane, where now the amplitude of the short-period variations has been reduced to avoid confusion. Not only is the final n_0/n_1 very close to the observed value, but the same is also seem for the eccentricity.

It is important to mention that not all tidal ejections result in smooth escapes. The crossing of the outer separatrix, present even for low eccentricities, introduces a chaotic behavior which, in some cases, led to an ejection in hyperbolic orbit or a collision of the planet with one of the stellar companions. Curiously, in other cases the planet's semimajor axis experienced a relatively small jump (of the order of ~ 0.1 AU) remaining bounded to the system and quickly attaining once again a near-circular orbit.

Figure 7 shows the results of a second N-body simulation, this time focusing on the ($n_0/n_1, e_1$) plane. We adopted the same system parameters as before, except for the tidal dissipation factor and mass of the planet, now chosen as $Q'_1 = 1$ and $m_1 = 20/3$. While seeming arbitrary, these give
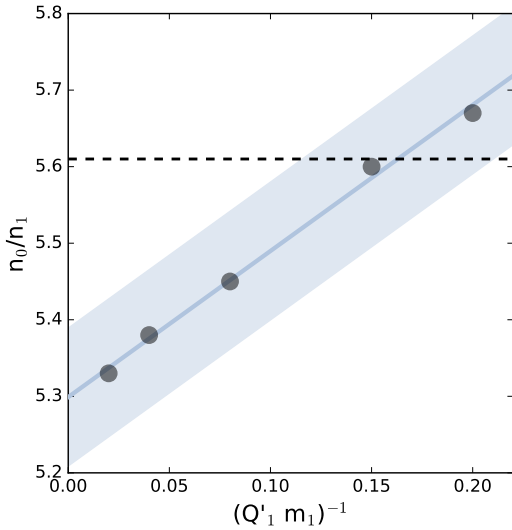
Figure 8. Filled circles indicate the final average n_0/n_1 attained after tidal evolution for T = 12.08 Gyrs for different values of $1/(Q'_1 m_1)$. Diagonal blue line is a linear fit of the data while the upper and low bounds represent the extent of the short period variations. Horizontal dashed line represents the current observed value of the mean-motion ratio.

the same factor $1/(Q'_1 m_1)$ and therefore lead to the same resonance divergence as seen in the first simulation. As before, the thick black curve shows the evolution of the orbit-averaged values while now the brown dots correspond to the full spread of osculating elements. A comparison with Figure 6 confirms that the final resting place of the system was the same in both cases.

As a test for the evolutionary path outside the mean-motion resonance, the dashed green line shows the forced eccentricity of the planet for each value of n_0/n_1, as given by:

$$e_f = \frac{5}{4}\left(\frac{m_{-1} - m_0}{m_{-1} + m_0}\right)\left(\frac{a_0}{a_1}\right)e_0 \qquad (15)$$

(Leung & Lee 2013), where in the plot we have taken into account the changes in binary eccentricity e_0 during the simulation. While initially the tidal evolution leads to higher values of e_1, these tend towards the secular forced eccentricity for increasing distance from the MMR. This lends additional credibility to our previous idea that the outward tidal migration of the planet is fueled by the effects of near-resonant effects on the secular solutions.

In Figure 8 we analyze how the final value of n_0/n_1, attained after the resonance capture and tidal evolution, depends on the factor $(Q'_1 m_1)$. Each filled circle shows the averaged value of the mean-motion ratio as obtained from a different simulation, while the blue thick line is a linear fit over all the data. The upper and lower limits of the light-blue region shows the extent of the short period oscillations. Since this magnitude is primarily dependent on the stellar masses, it is practically independent on the adopted values for the planetary parameters or initial conditions.

For $1/(Q'_1 m_1) \rightarrow 0$, corresponding to no tidal evolution of the planet, the final value of the mean-motion ratio tends to that solely defined by the stellar tides which, for

the adopted values of Q'_{-1} and Q'_0, is close to $n_0/n_1 \simeq 5.3$. Thus, in order to reach the observed resonance offset (horizontal dashed line) the planetary tide must have been the dominant driving mechanism, with values of the planetary parameters bounded by $(Q'_1 m_1) \lesssim 9$. Larger values (implying either larger planetary mass or tidal dissipation factor) would lead to n_0/n_1 closer to exact resonance and thus inconsistent with the current orbital configuration.

This limit on the factor $(Q'_1 m_1)$ is very strict and not easy to comply with. Adopting $m_1 \simeq 8m_\oplus$, as predicted by the mass-radius relationship of Mills & Mazeh (2017), implies Q'_1 of the order of unity, while usual estimations for the tidal parameter of rocky bodies is of the order of $10^1 - 10^2$ (e.g. Ferraz-Mello 2013). Even if the planetary mass were to be lower than the mean predicted value, it is difficult to imagine a scenario that could lead to significantly larger values of Q'_1.

However, as pointed out by Papaloizou (2015) citing the work by Ojakangas & Stevenson (1986), values closer to unity may be expected for small planets close to the solidus temperature, as expected during the first stages of post-formation evolution. Since we did not analyze the possibility of time-dependent Q'_1 in our simulations, nor is it clear how to accomplish such a task, we cannot vouch for the probability of this hypothesis.

5   SUMMARY AND DISCUSSION

In this work we presented a series of dynamical maps and N-body simulations whose aim was to study the dynamics of the 5/1 MMR in circumbinary systems, with special emphasis on the capture process through disk-planet interactions and the effects of tidal forces on the resonant motion. We found that the 5/1 mean-motion commensurability appears to have a complex structure with different libration modes (dubbed $(0, 0)$ and (π, π)) and even chaotic librations which are nonetheless orbitally stable for timescales of the order of Gyrs. These structures seem to be a strong function of the binary eccentricity and planetary masses, although we cannot rule out additional dependence on the stellar masses and (even) migration rates.

We applied these findings to the case of the Kepler-38 system and analyzed whether the present-day configuration could be explained by this combined process of resonance capture and tidal ejection. We chose Kepler-38 as a test for two main reasons: (i) capture in 5/1 mean-motion resonance has already been reported in this system with hydrodynamical simulations (Kley & Haghighipour 2014), and (ii) the system is very compact and sufficiently evolved (Orosz et al. 2012) so as to assume that tidal effects should have played an important role. Thus our model also included the past tidal evolution of the stars themselves.

For moderate primordial eccentricities of the binary, we found that resonance capture is highly probable in Kepler-38 system. In addition, the stability of the capture is guaranteed for extremely long time-spans, independently of the adopted planetary mass. This result is in contrast with what is suggested in Kley & Haghighipour (2014), where unstable behavior was expected soon after the dissipation of the disk.

N-body simulations of tidal evolution of the captured orbits showed that, contrary to expectations, the semimajor

axis of the planet increases with time independently of Q'_1, and even in a pseudo-synchronous configuration. We believe this behavior is related to the effects of near-resonant terms on the secular aligned-mode, although we cannot at present rule out the existence of a locus of resonant periodic orbits that could also drive the orbit outwards. Further studies into the structure of the 5/1 resonance are necessary before confirming any of these hypothesis.

The outward tidal migration of the planet, added to the orbital tidal decay of the binary, lead to an increase of the mean-motion ratio n_0/n_1. We then proceeded to estimate what combination of system parameters could yield final orbital separations consistent with the current values. For planetary masses similar to those predicted by recent mass-radius relations, we found that the tidal parameter of the planet must be very small, of the order of unity. While current tidal theories suggest values one or two orders of magnitude larger, very little is known about the dependence of Q' on the internal structure of the planets an even as a function of time. Thus, although this result does not help us to establish the capture/escape scenario as probable for Kepler-38, we cannot rule it out completely and perhaps future (and more precise) tidal models will shed more light on this issue.

Finally, although planetary scattering has recently been proposed as an alternative mechanism to explain the orbital architecture of some circumbinary planets (e.g. Gong & Ji 2017), the proximity of the observed eccentricity of Kepler-38 to its forced value makes this hypothesis unlikely for this system.

ACKNOWLEDGEMENTS

REFERENCES

Baran, A. S., Zola, S., Blokesz, A., Østensen, R. H., & Silvotti, R. 2015, A&A, 577, A146.

Batygin, K., & Morbidelli, A. 2013, AJ, 145, 1.

Beaugé, C. 1994, CeMDA, 60, 225.

Beaugé, C., Michtchenko, T. A., & Ferraz-Mello, S. 2006, MNRAS, 365, 1160.

Beaugé, C., & Nesvorný, D. 2012, ApJ, 751, 119.

Benítez-Llambay, P., Masset, F., & Beaugé, C. 2011, A&A, 528, A2.

Bowers, R. L., & Deeming, T. (1984). Astrophysics. Volume 1-Stars. Research supported by the University of Texas, Los Alamos National Laboratory, and Digicon Geophysical Corp. Boston, MA, Jones and Bartlett Publishers, Inc., 1984, 378 p.

Carpino, M., Milani, A., & Nobili, A. M. 1987, A&A, 181, 182.

Correia, A. C. M., Laskar, J., Farago, F., & Boué, G. 2011, CeMDA, 111, 105.

Correia, A. C. M., Boué, G., & Laskar, J. 2016, CeMDA, 126, 189.

Cresswell, P., & Nelson, R. P. 2006, A&A, 450, 833.

Cresswell, P., & Nelson, R. P. 2008, A&A, 482, 677.

D'Angelo, G., & Lubow, S. H. 2010, ApJ, 724, 730.

Delisle, J.-B., Laskar, J., Correia, A. C. M., & Boué, G. 2012, A&A, 546, A71.

Delisle, J.-B., Laskar, J., & Correia, A. C. M. 2014, A&A, 566, A137.

Dotter, A., Chaboyer, B., Jevremović, D., et al. 2008, ApJS, 178, 89-101.

Doyle, L. R., Carter, J. A., Fabrycky, D. C., et al. 2011, Science, 333, 1602.

Dunhill, A. C., & Alexander, R. D. 2013, MNRAS, 435, 2328.

Essick, R., & Weinberg, N. N. 2016, ApJ, 816, 18.

Ferraz-Mello, S. 2013, CeMDA, 116, 109.

Gallardo, T. 2006, Icarus, 184, 29.

Goldreich, P., & Schlichting, H. E. 2014, AJ, 147, 32.

Gong, Y., & Ji, J. 2017, AJ, 154, 179.

Hut, P. 1981, A&A, 99, 126.

Kley, W., & Haghighipour, N. 2014, A&A, 564, A72.

Kostov, V. B., McCullough, P. R., Hinse, T. C., et al. 2013, ApJ, 770, 52.

Kostov, V. B., McCullough, P. R., Carter, J. A., et al. 2014, ApJ, 784, 14.

Kostov, V. B., Orosz, J. A., Welsh, W. F., et al. 2016, ApJ, 827, 86.

Lee, M. H., & Peale, S. J. 2002, ApJ, 567, 596.

Lee, M. H., Fabrycky, D., & Lin, D. N. C. 2013, ApJ, 774, 52.

Leung, G. C. K., Lee, M. H. 2013, ApJ, 763, 107.

Leiva, A. M., Correa-Otto, J. A., Beaugé, C. 2013, MNRAS, 436, 3772.

Lines, S., Leinhardt, Z. M., Paardekooper, S., Baruteau, C., & Thebault, P. 2014, ApJ, 782, L11.

Lissauer, J. J., Ragozzine, D., Fabrycky, D. C., et al. 2011, ApJS, 197, 8.

Lithwick, Y., & Wu, Y. 2012, ApJ, 756, L11.

Maciejewski, G., Dimitrov, D., Fernández, M., et al. 2016, A&A, 588, L6.

Marzari, F., Thebault, P., Scholl, H., Picogna, G., & Baruteau, C. 2013, A&A, 553, A71.

Masset, F. S., Morbidelli, A., Crida, A., & Ferreira, J. 2006, ApJ, 642, 478.

Meschiari, S. 2012, ApJ, 752, 71.

Michtchenko, T. A., Malhotra, R. 2004, Icarus, 168, 237.

Mignard, F. 1979, Moon and Planets, 20, 301.

Mignard, F. 1980, Moon and Planets, 23, 185.

Mills, S. M., & Mazeh, T. 2017, ApJ, 839, L8.

Müller, T. W. A., & Kley, W. 2012, A&A, 539, A18.

Nelson, R. P. 2003, MNRAS, 345, 233.

Ojakangas, G. W., Stevenson, D. J. 1986, Icaurs, 66, 341.

Orosz, J. A., Welsh, W. F., Carter, J. A., et al. 2012, ApJ, 758, 87.

Orosz, J. A., Welsh, W. F., Carter, J. A., et al. 2012, Science, 337, 1511.

Papaloizou, J. C. B., & Terquem, C. 2010, MNRAS, 405, 573.

Papaloizou, J. C. B. 2011, CeMDA, 111, 83.

Papaloizou, J. C. B. 2015, Iinternational Journal of Astrobiology, 14, 291.

Paardekooper, S.-J., Leinhardt, Z. M., Thébault, P., & Baruteau, C. 2012, ApJ, 754, L16.

Pierens, A., & Nelson, R. P. 2007, A&A, 472, 993.

Pierens, A., & Nelson, R. P. 2008, A&A, 483, 633.

Pierens, A., & Nelson, R. P. 2013, A&A, 556, A134.

Ramos, X. S., Correa-Otto, J. A., & Beaugé, C. 2015, CeMDA, 123, 453.

Richardson, D. L., Kelly, T. J. 1988, CeMDA, 43, 193.

Rodet, L., Beust, H., Bonnefoy, M., et al. 2017, A&A, 602, A12.

Rodriguez, A., Ferraz-Mello, S., Michtchenko, T.A., Beaugé, C., & Miloni, O. 2011, MNRAS, 415, 2349.

Tanaka, H., Takeuchi, T., & Ward, W. R. 2002, ApJ, 565, 1257.

Tanaka, H., & Ward, W. R. 2004, ApJ, 602, 388.

12   *F.A. Zoppetti et al.*

Welsh, W. F., Orosz, J. A., Carter, J. A., et al. 2012, Nature, 481, 475.

Welsh, W. F., Orosz, J. A., Short, D. R., et al. 2015, ApJ, 809, 26.